*Trans ASME, Journal of Engineering Materials and Technology, **122** (2000) 129-134.*
(Journal's reprint is unavailable at this stage.)

ON THE LIMIT OF SURFACE INTEGRITY OF ALUMINA BY DUCTILE-MODE GRINDING

I. Zarudi and L. C. Zhang[1]

Department of Mechanical and Mechatronic Engineering

The University of Sydney, NSW 2006, Australia

[1] **Member of ASME and author for correspondence**

Trans ASME, Journal of Engineering Materials and Technology, ***122*** *(2000) 129-134.*
(Journal's reprint is unavailable at this stage.)

ABSTRACT

This paper investigates both experimentally and theoretically the formation mechanism of the surface integrity of alumina by ductile-mode grinding. It found that the distribution of the fractured area on a ground mirror surface, with the Rms roughness in the range from 30 nm to 90 nm, depends not only on the grinding conditions but also the pores in the bulk material. Surface pit formation is the result of interaction of abrasive impacts with pores. Thus the surface integrity achievable by ductile-mode grinding is limited by the initial microstructure of a material. The investigation shows that median and radial cracks do not exist and hence are not the cause of fracture as usually thought.

Keywords

Limit of surface integrity, ultra-precision grinding, alumina, grain size effect.

1. Introduction

High surface integrity of hard, brittle materials with perfect mirror-like and fracture-free surfaces of monocrystalline materials can be achieved by ultra-precision grinding (Zarudi and Zhang, 1997a, Suzuki, 1997). It has been shown theoretically and experimentally that the mechanism of material removal can be purely ductile when sufficient number of independent slip systems are activated (Zarudi and Zhang, 1997b). However, in the case of grinding polycrystals certain amount of fractured surface areas always appears causing the degradation of its surface integrity (Zarudi and Zhang, 1997b, Komanduri, 1996). This leads to controversial opinions on the nature of these fractured surface areas. For example, one has considered that the cause of such surface fracture could be the result of dislodgments of grains (Komanduri, 1996), or of the median and radial cracks developed in the subsurface (Bifano et al., 1991). Recently Tele (Tele, 1995) admitted that manufacturing defects such as pores or voids could also contribute to the surface integrity in machining.

The present study aims to explore the real cause of surface fracture of alumina through an investigation into the mechanisms of surface integrity formation in ultra-precision grinding.

Experiment

Polycrystalline alumina of 99.99 % purity produced by (Kyocera, Japan) with grain size of 1 μm and 25 μm were ground with an ultra-precision grinder, A modified Minini Junior 90 CF CNC M286 (measured loop stiffness = 80 N/μm). The grinding parameters used are listed in Tables 1 to 3.

The properties of a ground surface were explored by means of High Resolution Scanning Electron Microscope (HRSEM) JSM-6000F and Atomic Force Microscope (AFM). The subsurface structure of ground specimens was studied by Transmission Electron Microscope (TEM) EM 430. Cross-section view samples were made by the method proposed by Zarudi et al. (1996).

3. Results and Discussion

3.1. Material porosity before grinding

Pores were detected in both types of alumina before grinding. The amount of pores was determined by the technique of image analysis. It showed that pores in the 25 μm-grained alumina with an average diameter of 2 μm covered 5 % to 8 % of the whole ground surface and those in the 1 μm-grained alumina featuring an average diameter of 0.3 μm covered 1 % to 2 % of the ground surface.

3.2 Surface topography after grinding

Typical topography of ground surfaces is shown in **Fig.1**. Mirror surfaces were generated under all the table speeds listed in Table 1. Grooves could be clearly observed under AFM **Fig 1(a, c)**. However, some pits were also observed **Fig1(b, e)**. The values of Rms roughness *vs* table speed for both types of alumina are shown in **Fig.2**. It is clear that the Rms roughness increases with the increase of table speed. For the 1 μm-grained alumina the Rms roughness grows from 30 nm to 50 nm when the table speed changes from 0.02 m/min to 1 m/min. For the 25 μm-grained alumina, it increased from 33 nm to 88 nm and

thus the effect was greater. Clearly, surface roughness must be affected by the surface pits. In the parts without pits Rms roughness was only between 15 nm and 20 nm.

The surface areas covered by pits (SACP) were also determined by the technique of image analysis, as shown in **Fig.3**. It is obvious that the SACP decreases significantly when the table speed of grinding decreases. In other words, SACP becomes smaller if the nominal chip thickness in grinding is smaller. Furthermore, the percentage of SACP on the ground surface of the 1 μm-grained alumina is always much less than that on the ground surface of the 25 μm-grained alumina. In the range of table speed from 0.2 m/min to 0.5 m/min, the rate of increment of SACP on the 25 μm-grained alumina is quite high.

To study the nature of fractured surfaces of SACP we used HRSEM. The detailed topography of typical pits can be seen in **Fig.4**. The edges of the pits show obvious feature of fracture while the central parts of them resemble the characteristics of the cross-sections of pores. Under higher magnifications (**Fig.5**), it is clear that cracks appeared in the vicinity of pore edges (**Fig.5b**).

3.3 Subsurface structure

Before ultra-precision grinding, the damaged subsurface layer induced by specimen preparation (conventional grinding) was determined so that the initially damaged zone could be removed completely during the subsequent ultra-precision grinding. Thus in all the cases below the characterisation of the subsurface structure were purely caused by the ultra-precision grinding.

Figure 6 shows two distinguished regions in the subsurfaces of both types of alumina. The first region, which is immediately under the ground surface, is characterised by an extremely high density of dislocations. In the 25 μm-grained alumina, the depth of

the region is from 0.2 μm to 0.4 μm, depending on the table speed used. In the 1 μm-grained alumina it varies from 0.1 to 0.3 μm. The second region (**Fig.6**) is with a much lower density of dislocations and has a thickness of 0.2 μm to 0.5 μm in the 25 μm-grained alumina and of 0.1 μm to 0.2 μm in the 1 μm-grained alumina. No microcracks were found in the subsurface areas without pores. This means that in the areas without pores, material removal is under a real ductile-mode.

The crack-free behaviour in the first region can be explained by the nucleation of sufficient number of twin and slip systems (Chin, 1975), because in this region grinding created at least five independent such systems (Zarudi et al., 1997). The second zone has less than five independent slip and twin systems and thus microcracking should be highly possible there. However, this is inconsistent with the above experimental observations. Such phenomenon can be elucidated by the possibility of microcracking due to the pile-up of dislocations on an active slip plane. In fact, the threshold of an effective resolve shear stress (τ_s) for cracking can be determined by (Hagan, 1979):

$$\tau_s^2 = \frac{3\pi}{8}\left[\frac{\gamma\mu}{(1-\nu)L}\right] \tag{1}$$

where γ is the fracture surface energy, μ is shear modulus, ν is Poisson's ratio, and L is the length of pile-up. Considering that the length of pile-up in the above specimens (ie, penetration depth of dislocation in subsurface) was only from 150 nm to 500 nm, we can see from Eq.(1) that such a pile-up would lead to a high value of τ_s thus eliminate the nucleation of microcracks. In addition, it is worth to note that the interaction of different slip systems was a rear event in the second region because of the extremely low density of dislocations. Hence, no microcracks can be created via interaction.

From the above discussion, it is clear that the initiation of dislocations in subsurface does not create sufficient stress concentrators for microcracking. Equally

importantly, there are no median or radial cracks. These clearly indicate that the existing explanations about the formation of fractured surfaces are not suitable for understanding the SACP in ultra-precision grinding of alumina. Our following theoretical analysis can explain the fracture around pore edges and the variation of SACP on the ground surfaces of different types of alumina.

3.4 Grinding materials containing pores

For simplicity, we assume that forces in grinding are distributed equally among active abrasive grains in the grinding zone and that all grains have an equal diameter of 1 μm for the grinding wheel used in the present study. Experimentally determined forces listed in Table 4 can then be used in calculations. Using the method shown by Zhang et al., (1995) the number of active grains per micron in our experiment is found to be 2.5.

Following the approach used for impact loads (Galiev, 1996) we assume that the stress state in the material induced by abrasive impact is similar to that under an equivalent static load and that the shape of a pore is axisymmetrical about the normal of the ground surface. Thus in grinding a material containing pores, as shown in **Fig.7**, we encounter two cases, an abrasive grain interacting with a closed pore in the subsurface or with an open pore on the surface.

1. Closed pore in the 1 μm-grained alumina

In this case, the layer of alumina on the top of a pore can be modelled by a clamped circular plate with a variable thickness. The cross section of such plate model is shown in **Fig.8a**. At the peripheral part, the plate has a linearly varying thickness. The extension of line AB intersects with the top surface at centre O. The ratio b/a was taken as 0.8.

As the average radius of pores was only 0.3 μm in the 1 μm-grained alumina, interacting stress from a single grit is approximated by a uniform pressure over the whole plate with a diameter of 0.3 μm (equal to the average diameter of pores). The maximum bending moment of the plate can be written as (Timoshenko and Woinowsky-Krieger, 1976):

$$M_{\max} = M_0 - \frac{P}{8\pi} + \gamma_1 P \tag{2}$$

where

$$M_0 = \frac{P(1+\nu)a^2}{16} \tag{3}$$

P is the total load applied on a pore through an active abrasive grain, υ is Poisson's ratio and *a* is the radius of the plate. In Eq. (2) γ_1 is a function of b/a and can be taken as - 0.05 for b/a=0.8 (Timoshenko and Woinowsky-Krieger 1976).

2. A closed pore in the 25 μm-grained alumina

As the average radius of pores in the 25 μm-grained alumina is 2 μm, the diameter of the plate model is also taken to be 2 μm. The interacting stress in this case distributes only partially on the plate bounded by a circle of radius equal to 1 μm, the average diameter of abrasive grains, as shown in **Fig.8b**.

Under this loading condition, the maximum bending moment in the plate can be determined by (Timoshenko and Woinowsky-Krieger, 1976):

$$M_{\max} = M_0 - \frac{P}{4\pi}(1 - \frac{c^2}{2a^2}) + \gamma_1 P\,, \tag{4}$$

where

$$M_0 = \frac{P}{4\pi}\left[(1+\nu)\log\frac{a}{c} + 1 - \frac{(1-\nu)c^2}{4a^2}\right]. \tag{5}$$

3. An open pore

When a pore opens partially or fully to the grinding surface, the problem can be treated as a plate with a central hole subjected to an interacting stress from an abrasive grain, as shown in **Fig.8c**. The maximum bending moment in this case is (Timoshenko and Woinowsky-Krieger, 1976):

$$M_{\max} = \frac{P}{4\pi\left[(1+\nu)\frac{a^2}{d^2}+1-\nu\right]}\left[(1-\nu)(\frac{a^2}{d^2}-1)+2(1+\nu)\frac{a^2}{d^2}\log\frac{a}{d}\right], \qquad (6)$$

where d is radius of the hole.

On the other hand the stress intensity factor of a plate with voids can be expressed as (Rooke and Cartwrite, 1976):

$$K_1 = \frac{6M}{(h-g)^{3/2}} f(g/h), \qquad (7)$$

where M is the bending moment, h is the thickness of the plate in the central part and *g* is the length of a possible imperfections. Some imperfections always exist in ceramics, which can be grain boundaries, faults of structure etc. To be conservative, we took the smallest imperfection size of 15 nm assuming that the material is almost perfect.

The stress intensity factors obtained above can then be used to examine the fracture behaviour of alumina around pore edges. Assume that a fracture will take place when the stress intensity factor exceeds the corresponding fracture toughness, which is 0.7 $\mathrm{MPa}\times\mathrm{m}^{1/2}$ for the 25 μm-grained alumina and 2 $\mathrm{MPa}\times\mathrm{m}^{1/2}$ for the 1 μm-grained alumina (Xu, 1996).

Table 5 shows the critical thickness of the layer (h_c) above a pore. For instance, in grinding the 25 μm-grained alumina for a closed pore h_c is 200 nm under the table speeds of 0.02 m/min and 0.1 m/min. Thus microcracking will take place if the thickness of the

layer above a pore is less than 200 nm. Generally, h_c is smaller under lower table speeds, indicating that fracture initiation is harder. Thus under a lower table speed, the overall surface roughness will be smaller and SACP will also be smaller.

In the case with the 1 μm-grained alumina h_c is considerably smaller and is in the range from 20 to 50 nm when table speed varies. This explains why the microfracturing effect of pores in the 1 μm-grained alumina is much lower then that with the 25 μm-grained alumina as presented by **Fig.3**.

When a pore is open, edge fracture always exists since the edge thickness of the open pore is normally variable and is often less than h_c.

Clearly, the pore effect on microcracking limits the surface integrity achievable. Thus in ultra-precision grinding of polyscrystalline alumina containing pores, microcracking around pore edges always occurs, although a pure ductile-mode of material removal can be achieved by the activated slip and twin systems in the areas without pores.

Conclusions

1. The nature of SACP on ground surfaces is related to pores in the bulk material.
2. The subsurface structure of alumina after ultra-precision grinding is composed of a layer with a high density of dislocations and a layer with lower density of dislocations.
3. A real ductile-mode of material removal is possible due to the initiation of more than five independent slip and twin systems in the first layer. However, the absence of microcracks in the second layer is due to the small length of pile-ups that cannot create sufficiently high stresses to initiate microcracking.
4. No radial and lateral cracks appeared in the whole subsurface of alumina after ultra-precision grinding.

5. The existence of pores in alumina limits the level of the surface integrity achievable by ultra-precision grinding. The ultimate surface integrity is determined by the percentage and size of pores, but not only the depth of cut as usually thought.

ACKNOWLEDGMENTS

The authors wish to thank the Australian Research Council (ARC) for continuing support of this project. We thank also the Electron Microscope Unit for use of its facilities.

References

Bifano T. G., Dow T. A., Scattergood R. O., 1991, "Ductile-regime grinding: a new technology for machining brittle materials", *Transactions ASME J. of Engineering materials and Technology*, 113:184-189.

Chin G. Y., 1975, "Slip and twinning systems in ceramic crystals", in *Deformation of ceramic materials*, 1975, (eds) R. C. Brand and R. E. Tressler, 25-44.

Galiev S. U., 1996, "Experimental observations and discussion of counterintuitive behaviour of plates and shallow shells subjected to blast loading", *Int. J. Impact Eng*., 18:783-802.

Hagan T., 1979, "Micromechanics of crack nucleating during indentation", *J. Mat. Sci*., 14:2975-2980.

Komanduri R., 1996, "On material removal mechanisms in finishing of advanced ceramics and glasses", *Cirp Annals*, 45:09-514.

Rooke D. P. and Cartwrite D. J., 1976, *Compendium of stress-intensity factors*, Her Majesty's Stationery Office, London.

Suzuki H., Wajima N., Zahmaty M. S., Kuriyagava T., Syoji K.. "Precision grinding of a spherical surface accuracy improving by on-machine measurement.", in: *Advances in Abrasive Technology*, 1997, L. C. Zhang and N. Yasunaga, ed. (World Scientific, Singapore, 1997) 116-121.

Tele R., 1995, "Ceramography of high performance ceramics. Part IX: Pores and chips", *Prakt. Metallogr*, 32:440-466.

Timoshenko S. P. and Woinowsky-Krieger S., 1976, *Theory of plates and shells*, McGraw-Hill Book, Singapore.

Zarudi I. and Zhang L. C., 1997a, "Subsurface structure change of silicon after ultra-precision grinding", in: *Advances in Abrasive Technology*, L. C. Zhang and N. Yasunaga, ed. 33 (World Scientific, Singapore), 33-38.

Zarudi I., Zhang L. C., 1997b "Surface and subsurface structure of alumina after ductile mode grinding", Proc. of 12-th ASPE annual meeting, 267-270.

Zarudi I., 1996, "Plastic zone formation in alumina associated with ultra-precision grinding", *Proc. of the 11th ASPE*, 610-613.

Zarudi I., Zhang L. C. and Mai Y.-W., 1996,. "Subsurface damage in alumina induced by single-point scratching", *J. of Mater. Sci*., 31:905-914.

Zhang Bi, Howes T. D., 1995, 'Subsurface evaluation of ground ceramics", *Annals of CIRP*, 44:263-266.

Xu H. H. K., Wei L. and Jahanmir S., 1996, "Influence of grain size on the grinding response of alumina", *J. Am. Ceram. Soc*., **7**9:1307-1313.

Figure legends

Fig.1 Topography of surfaces after ductile-regime grinding: (a) and (b) the 1 μm-grained alumina; (c) and (d) the 25 μm-grained alumina; (a) and (c) 3-d image of the surface; (b) and (d) general view.

Fig.2 Effect of table speed on Rms roughness of alumina with different grain sizes.

Fig.3 Effect of table speed on surface area covered by pits.

Fig.4 Topography of pits: (a) the 1 μm-grained alumina, (b) the 25 μm-grained alumina.

Fig.5 Subsurface structure in the vicinity of a pit: (a) general view; (b) a detailed view of the pore edge with microcracks.

Fig.6 Subsurface structure of alumina after ultra-precision grinding: (a) the 1 μm-grained alumina, (b) the 25 μm-grained alumina.

Fig.7 Ductile-mode grinding of alumina containing pores.

Fig.8 Model for interaction between an abrasive grain and material containing pores:(a) and (b) closed pores, (c) an open pore; (a) the 1 μm-grained alumina, (b) the 25 μm-grained alumina.

Table legends

Table 1. Grinding conditions.

Table 2. Wheel dressing conditions.

Table 3. Wheel truing conditions.

Table 4. Measured grinding forces.

Table 5. Pore effect on microcracking in grinding

*Trans ASME, Journal of Engineering Materials and Technology, **122** (2000) 129-134.*
(Journal's reprint is unavailable at this stage.)

Zarudi I. and Zhang L. C. ON THE LIMIT OF SURFACE INTEGRITY OF ALUMINA

(a)

(b)

Fig.1

(c)

(d)

Fig.1

*Trans ASME, Journal of Engineering Materials and Technology, **122** (2000) 129-134.*
(Journal's reprint is unavailable at this stage.)

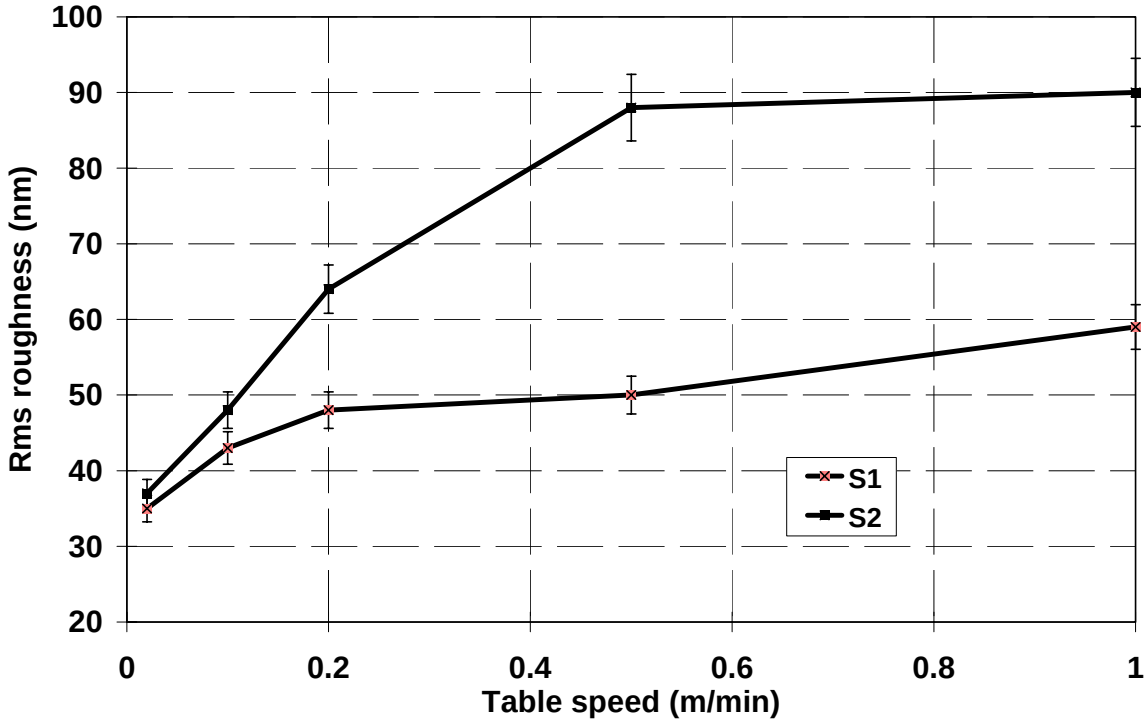

Fig.2

*Trans ASME, Journal of Engineering Materials and Technology, **122** (2000) 129-134.*
(Journal's reprint is unavailable at this stage.)

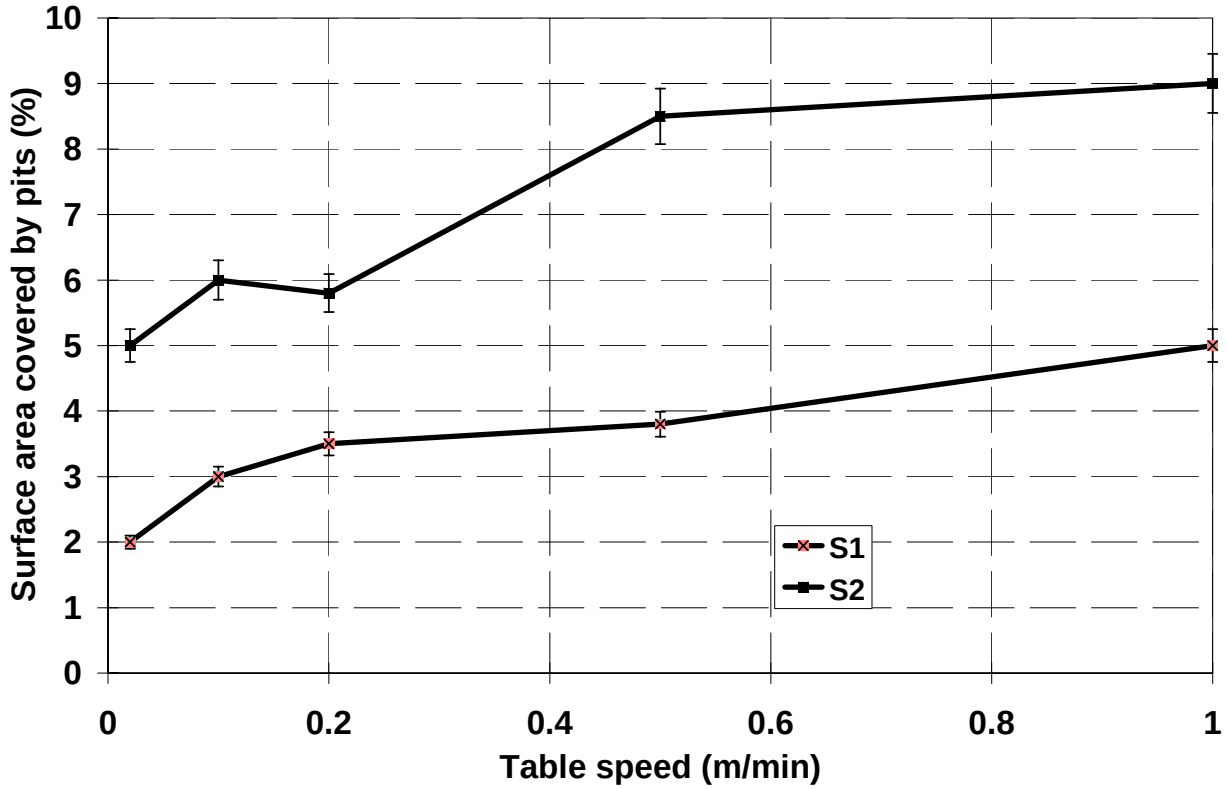

Fig.3

(a)

(b)

Fig.4

(a)

(b)

Fig.5

Zarudi I. and Zhang L. C. ON THE LIMIT OF SURFACE INTEGRITY OF ALUMINA

(a)

(b)

Fig.6

*Trans ASME, Journal of Engineering Materials and Technology, **122** (2000) 129-134.*
(Journal's reprint is unavailable at this stage.)

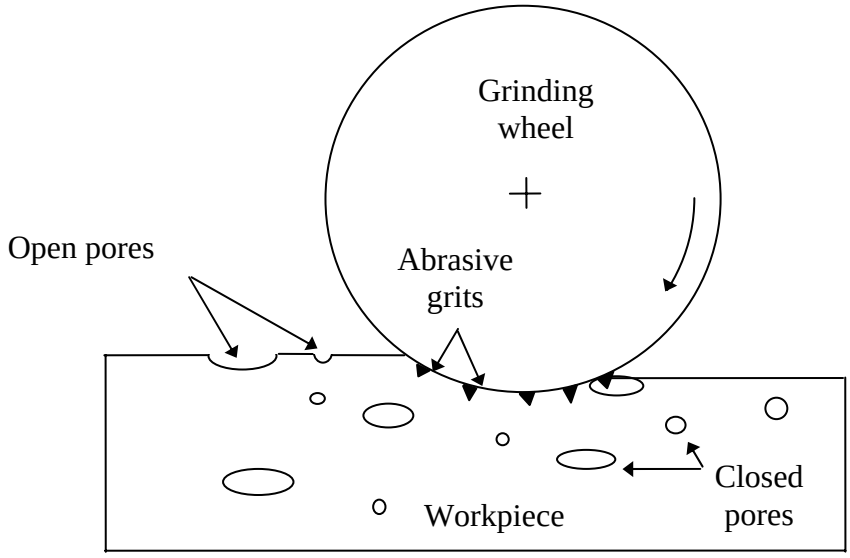

Fig.7

*Trans ASME, Journal of Engineering Materials and Technology, **122** (2000) 129-134.*
(Journal's reprint is unavailable at this stage.)

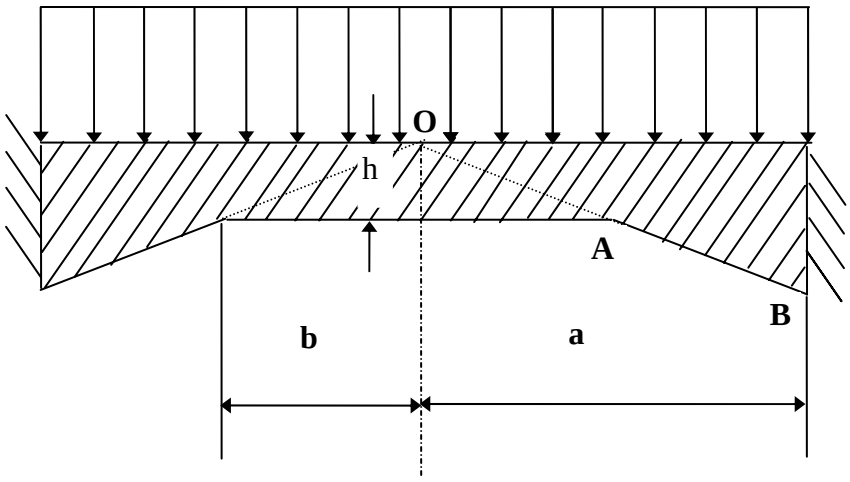

(a)

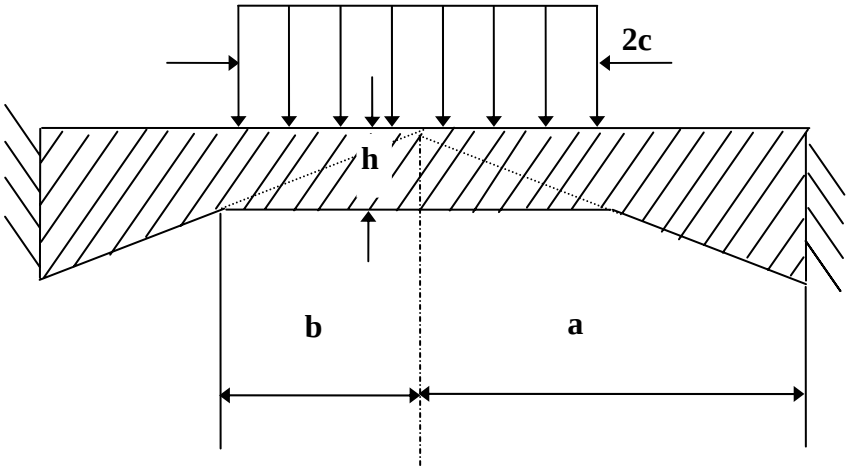

(b)

Fig.8

*Trans ASME, Journal of Engineering Materials and Technology, **122** (2000) 129-134.*
(Journal's reprint is unavailable at this stage.)

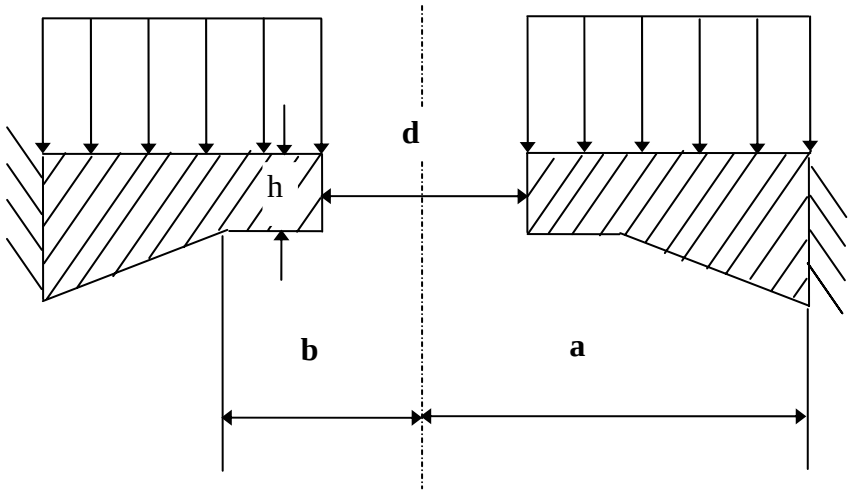

(c)

Fig.8

*Trans ASME, Journal of Engineering Materials and Technology, **122** (2000) 129-134.*
(Journal's reprint is unavailable at this stage.)

Table 1.

Workpiece material	Polycrystalline alumina 1 μm grained and 25 μm grained.
Grinding wheel	SD4000L75BPF
Wheel diameter (mm)	305
Wheel speed (m/s)	27
Grinding width (mm)	5
Table speed (m/min)	0.02; 0.1; 0.2; 0.5; 1
Depth of cut (nm)	100
Coolant	Syntilo 3 (99 % water, 1% mineral oil)

Table 2.

Type of dresser	Multipoint diamond
Radial feed (mm × str)	0.05 × 5 + 0.02 × 1
Wheel speed (m/min)	10
Dressing, cross-feed rate (mm/rev)	0.01

Table 3.

Truing procedure	Feeding of a pyrex lap
Diameter of diamond abrasive in paste (μm)	1
Wheel speed (m/min)	5
Truing cross-feed rate (mm/rev)	0.01

Table 4.

Type of alumina	Table speed (m/min)	Normal force (N/mm)	Tangential force (N/mm)
the 1 μm grained	0.02	40	1.7
	0.1	33	1.3
	0.2	32	1.28
	0.5	25	1.2
	1	20	0.8
the 25 μm grained	0.02	1.2	0.06
	0.1	1.8	0.1
	0.2	2	0.1
	0.5	2.2	0.1
	1	2.6	0.13

Table 5.

Type of alumina	Table speed (m/min)	Critical thickness of material above a pore h_c (nm)	
		Closed pore	Open pore
the 25 μm-grained	0.02	200	50
	0.1	200	50
	0.2	250	100
	0.5	300	100
	1	300	100
the 1 μm-grained	0.02	50	100
	0.1	50	50
	0.2	50	50
	0.5	20	20
	1	20	20